Flow and Heat Transfer Characteristics of Turbulent Gas Flow in Microtube with Constant Heat Flux

Flow and Heat Transfer Characteristics of Turbulent Gas Flow in Microtube with Constant Heat Flux

Chungpyo Hong[1], Yutaka Asako[2], Shinichi Matsushita[1] and Ichiro Ueno[1]
[1]Dept. of Mechanical Engineering, Tokyo University of Science, Chiba, Japan
[2]Dept. of Mechanical Engineering, Tokyo Metropolitan University, Tokyo, Japan

E-mail: hong@rs.noda.tus.ac.jp

Abstract. Local friction factors for turbulent gas flows in circular microtubes with constant wall heat flux were obtained numerically. The numerical methodology is based on arbitrary-Lagrangian-Eulerian method to solve two-dimensional compressible momentum and energy equations. The Lam-Bremhorst's Low-Reynolds number turbulence model was employed to calculate eddy viscosity coefficient and turbulence energy. The simulations were performed for a wide flow range of Reynolds numbers and Mach numbers with different constant wall heat fluxes. The stagnation pressure was chosen in such a way that the outlet Mach number ranged from 0.07 to 1.0. Both Darcy friction factor and Fanning friction factor were locally obtained. The result shows that the obtained both friction factors were evaluated as a function of Reynolds number on the Moody chart. The values of Darcy friction factor differ from Blasius correlation due to the compressibility effects but the values of Fanning friction factor almost coincide with Blasius correlation. The wall heat flux varied from 100 to 10000 W/m^2. The wall and bulk temperatures with positive heat flux are compared with those of incompressible flow. The result shows that the Nusselt number of turbulent gas flow is different from that of incompressible flow.

1. Introduction

The number of applications of micro-electro mechanical systems (MEMS) has increased the need for understanding heat transfer in micro-geometries. In the case of micro-tube gas flows, it is found that the flow accelerates due to the gas expansion and thermal energy converts to kinetic energy. This results in a static temperature decrease of the gas [1].
Since the experimental work by Wu and Little [2], who measured the friction coefficient and Nusselt number for nitrogen, argon and helium flows in silicon or glass micro-channels, many experimental and numerical investigations have been undertaken.
Chen and Kuo [3] solved numerically the compressible turbulent boundary layer equations with using Baldwin-Lomax model. Their calculated friction factor is higher than that of Blasius correlation and calculated temperature dropped well below the wall temperature at the outlet due to energy conversion into the kinetic energy.
Hara et al. [4] experimentally investigated heat transfer for high pressure ratio of air flow in square mini-channels whose size was 0.3 to 2.0 mm and length was 10 mm to 100 mm. They reported that

Address correspondence to Dr. Chungpyo Hong, Dept. of Mechanical Engineering, Tokyo University of Science, 2641 Yamazaki, Noda, Chiba 278-8510, Japan. E-mail:hong@rs.noda.tus.ac.jp

the heat transfer coefficient was about 7.3 times greater than Dittus and Boelter correlation for fully developed turbulent pipe flow.

Turner et al. [5] performed experimental investigations to measure the inlet and outlet temperatures and the micro-channel wall temperature in thermal boundary conditions of constant temperature gradient along the micro-channel length. The experimental measurements of the inlet and outlet gas temperature and the micro-channel wall temperature were used to validate a two dimensional numerical model for the laminar gaseous flow in micro-channel. Asako [6], Asako and Toriyama [7] and Hong and Asako [8] performed numerical investigations to obtain the heat transfer characteristics of laminar gas flows in a micro-channel and in a micro-tube with constant wall temperature, whose wall temperature is lower or higher than the inlet temperature. In the case of slow flow (Ma_{out}<0.3), identical heat transfer coefficients are obtained for both heated and cooled cases. However, in the case of fast flow, different heat transfer coefficients are obtained for each cooled and heated case. The way to predict of the heat transfer rate of gaseous flow in a micro-channel and in a micro-tube has been proposed.

Recently, Hong et al. [9] measured total temperatures at the outlet of a micro-tube of D=163-242 μm with constant wall temperature whose temperature is higher than the inlet temperature in the laminar flow regime in order to validate numerical results by Hong and Asako [8]. The bulk temperatures obtained experimentally are in excellent agreement with those of numerical results. They found that measured total temperatures at the outlet are higher than the bulk temperatures of incompressible due to the additional heat transfer from the wall to the gas.

Chen et al. [10] investigated experimentally forced convective heat transfer characteristics of air and CO_2 in micro stainless steel tube with inside diameter of 920 μm. The tube wall was heated by electric current. They used a non-contacted liquid crystal thermography (LCT) temperature measurement method and thermocouples to measure the surface temperature of micro-tube. They concluded that the conventional heat transfer correlation of laminar and turbulent flow can be well applied for prediction of heat transfer performance in a micro-tube. However, Yang et al. [11] investigated experimentally and numerically the characteristics of nitrogen gas convective heat transfer in commercial stainless steel micro tubes with inner diameter of 175μm and 750 μm.

Hong et al. [12] and Isobe et al. [13] investigated experimentally heat transfer characteristics of turbulent gas flow in micro tube with constant wall temperature. The experiments were performed for nitrogen gas flow through a micro-tube with 243 μm and 342 μm in diameter and 50 mm in length. The wall temperature was maintained at 310-350 K. They reported that heat transfer characteristics of turbulent gas flow in micro-tube with constant wall temperature are different from those of the incompressible flow. Additional heat transfer for turbulent flow is more dominant than that for laminar flow.

As can be seen from the literature survey, there seems to be few numerical investigations on the heat transfer of turbulent gas flow though a micro-tube. Chen and Kuo [3] numerically investigated the heat transfer of turbulent gas flow through a micro-tube. However, in their paper, the effect of compressibility on turbulent heat transfer is not clear. Therefore, in turbulent flow regime the effect of compressibility on heat transfer has not been clarified totally yet. This has motivated the present numerical study to obtain heat transfer characteristics of turbulent gas flow in microtubes with constant heat flux.

2. Formulation

2.1. Description of the problem and conservation equations

The problem modelled in this study is depicted schematically in Figure. 1. The characteristics of turbulent gas flow in a microtube will be determined. A reservoir at the stagnation temperature, T_{stg}, and the stagnation pressure, p_{stg}, is attached to the upstream section of the microtube. The gas flows into the microtube and flows out to atmosphere. The wall temperature of the tube is assumed to be constant. The

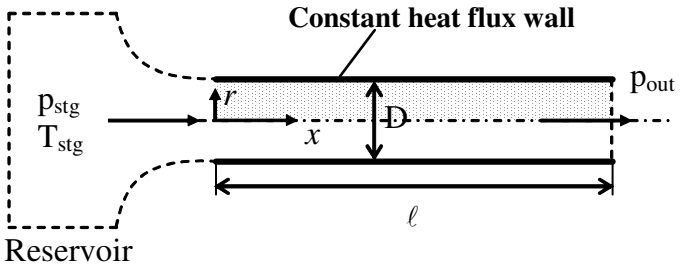

Fig. 1 Schematic diagram of problem

flow assumed to be steady, axisymmetric and turbulent. Two-dimensional coordinates are used for computations. The fluid is assumed to be an ideal gas. The governing equations to be considered are the time-averaged compressible continuity, momentum, and energy equations [14]. An eddy viscosity model is used to account for the effect of turbulence. The model chosen is the Lam-Bremhorst low-Reynolds number form of the k-ε (turbulence kinetic energy-turbulence dissipation rate) model [15]. Constant thermophysical properties are assumed. The Reynolds stress of compressible flow is modeled by

$$-\overline{\rho u_i' u_j'} = \mu_t\left\{\left(\frac{\partial \tilde{u}_i}{\partial x_j}+\frac{\partial \tilde{u}_j}{\partial x_i}\right)-\frac{2}{3}\delta_{ij}\frac{\partial \tilde{u}_k}{\partial x_k}\right\}-\frac{2}{3}\delta_{ij}\bar{\rho}\tilde{k} \tag{1}$$

The governing equations can be expressed as

$$\frac{\partial \bar{\rho}\tilde{u}}{\partial x}+\frac{1}{r}\frac{\partial \bar{\rho} r\tilde{v}}{\partial r}=0 \tag{2}$$

$$\frac{\partial \bar{\rho}\tilde{u}\tilde{u}}{\partial x}+\frac{1}{r}\frac{\partial \bar{\rho} r\tilde{u}\tilde{v}}{\partial r}=-\frac{\partial}{\partial x}\left(\bar{p}+\frac{2}{3}\bar{\rho}k\right)+\frac{\partial \tau_{xx}}{\partial x}+\frac{1}{r}\frac{\partial}{\partial r}\left(r\tau_{rx}\right) \tag{3}$$

$$\frac{\partial \bar{\rho}\tilde{u}\tilde{v}}{\partial x}+\frac{1}{r}\frac{\partial \bar{\rho} r\tilde{v}\tilde{v}}{\partial r}=-\frac{\partial}{\partial r}\left(\bar{p}+\frac{2}{3}\bar{\rho}k\right)+\frac{\partial \tau_{rx}}{\partial x}+\frac{1}{r}\frac{\partial}{\partial r}\left(r\tau_{rr}\right)-\frac{\tau_{\theta\theta}}{r} \tag{4}$$

$$\frac{\partial \bar{\rho}\tilde{u}\tilde{i}}{\partial x}+\frac{1}{r}\frac{\partial \bar{\rho} r\tilde{v}\tilde{i}}{\partial r}=-\left(\bar{p}+\frac{2}{3}\bar{\rho}K\right)\left(\frac{\partial \tilde{u}}{\partial x}+\frac{1}{r}\frac{\partial r\tilde{v}}{\partial r}\right)+\frac{\partial}{\partial x}\left\{\left(\lambda+\lambda_t\right)\frac{\partial \tilde{T}}{\partial x}\right\}+\frac{1}{r}\frac{\partial}{\partial r}\left\{\left(\lambda+\lambda_t\right)r\frac{\partial \tilde{T}}{\partial r}\right\}+\left(\mu+\mu_t\right)\phi \tag{5}$$

where the components of viscous stress tensor are

$$\begin{aligned}&\tau_{xx}=\left(\mu+\mu_t\right)\left\{2\frac{\partial \tilde{u}}{\partial x}-\frac{2}{3}\left(\frac{\partial \tilde{u}}{\partial x}+\frac{1}{r}\frac{\partial r\tilde{v}}{\partial r}\right)\right\},\quad \tau_{xr}=\tau_{rx}=\left(\mu+\mu_t\right)\left(\frac{\partial \tilde{v}}{\partial x}+\frac{\partial \tilde{u}}{\partial r}\right)\\&\tau_{rr}=\left(\mu+\mu_t\right)\left\{2\frac{\partial \tilde{v}}{\partial r}-\frac{2}{3}\left(\frac{\partial \tilde{u}}{\partial x}+\frac{1}{r}\frac{\partial r\tilde{v}}{\partial r}\right)\right\},\quad \tau_{\theta\theta}=\left(\mu+\mu_t\right)\left\{2\frac{\tilde{v}}{r}-\frac{2}{3}\left(\frac{\partial \tilde{u}}{\partial x}+\frac{1}{r}\frac{\partial r\tilde{v}}{\partial r}\right)\right\}\end{aligned} \tag{6}$$

ϕ is dissipation function described as follows

$$\phi=2\left[\left(\frac{\partial \tilde{u}}{\partial x}\right)^2+\left(\frac{\tilde{v}}{r}\right)^2+\left(\frac{\partial \tilde{v}}{\partial r}\right)^2\right]-\frac{2}{3}\left(\frac{\partial \tilde{u}}{\partial x}+\frac{1}{r}\frac{\partial r\tilde{v}}{\partial r}\right)^2+\left(\frac{\partial \tilde{v}}{\partial x}+\frac{\partial \tilde{u}}{\partial r}\right)^2 \tag{7}$$

Furthermore, the working gas is assumed to be an ideal gas so that the equation of state is valid

$$\tilde{i}=\frac{R}{\gamma-1}\bar{T}=\frac{1}{\gamma-1}\frac{\bar{p}}{\bar{\rho}} \tag{8}$$

2.2. Turbulence model

In *k*-ε turbulence model, turbulence kinetic energy *k* and viscosity coefficient μ_t are determined solving the equations of transportation below

$$\frac{\partial \bar{\rho}\tilde{u}k}{\partial x}+\frac{1}{r}\frac{\partial \bar{\rho}r\tilde{v}k}{\partial r}=\frac{\partial}{\partial x}\left\{\left(\mu+\frac{\mu_t}{\sigma_k}\right)\frac{\partial k}{\partial x}\right\}+\frac{1}{r}\frac{\partial}{\partial r}\left\{\left(\mu+\frac{\mu_t}{\sigma_k}\right)r\frac{\partial k}{\partial r}\right\}+(P)_k-\bar{\rho}\varepsilon \tag{9}$$

$$\frac{\partial \bar{\rho}\tilde{u}\varepsilon}{\partial x}+\frac{1}{r}\frac{\partial \bar{\rho}r\tilde{v}\varepsilon}{\partial r}=\frac{\partial}{\partial x}\left\{\left(\mu+\frac{\mu_t}{\sigma_\varepsilon}\right)\frac{\partial \varepsilon}{\partial x}\right\}+\frac{1}{r}\frac{\partial}{\partial r}\left\{\left(\mu+\frac{\mu_t}{\sigma_\varepsilon}\right)r\frac{\partial \varepsilon}{\partial r}\right\}+c_1f_1\frac{\varepsilon}{k}P_k-c_2f_2\bar{\rho}\frac{\varepsilon^2}{k} \tag{10}$$

$$P_k=\mu_t\varphi-\frac{2}{3}\bar{\rho}k\left(\frac{\partial \tilde{u}}{\partial x}+\frac{1}{r}\frac{\partial r\tilde{v}}{\partial r}\right) \tag{11}$$

$$\mu_t=C_\mu f_\mu\bar{\rho}\frac{k^2}{\varepsilon} \tag{12}$$

The various ways have been presented to model the coefficients appearing these equations [16]. In this paper, the Lam- Bremhorst low Reynolds number model was adopted and the
following values are used for coefficients

$$C_\mu=0.09,\quad \sigma_k=1.0,\quad \sigma_\varepsilon=1.3,\quad C_1=1.44,\quad C_2=1.92 \tag{13}$$

$$f_1=1+\left(\frac{0.05}{f_\mu}\right)^3,\quad f_2=1-e^{-Rt^2}\quad f_\mu=\left(1-e^{-0.0165R_y}\right)^2\left(1+\frac{20.5}{R_T}\right) \tag{14}$$

$$R_T=\frac{\bar{\rho}k^2}{\varepsilon\bar{\mu}},\qquad R_y=\frac{\bar{\rho}\sqrt{k}y_W}{\bar{\mu}} \tag{15}$$

where y_W is defined as the minimum distance from the tube wall. Turbulent thermal conductivity in Eq. (5) is

$$\lambda_t=\frac{c_p\mu_t}{Pr_t} \tag{16}$$

where Pr_t is the turbulent Prandtl number and its value is 0.9.

2.3. Boundary conditions

In the range of the micro tube sizes considered in this paper, Knudsen number is less than 0.001 for the atmospheric pressure and the room temperature so that the effect of rarefaction can be neglected. Therefore no-slip condition at the wall is used for velocity. Also, it is assumed that the tube wall is constant heat flux and at the tube inlet the distributions of velocity, pressure, temperature and density are uniform. From the assumptions above, the boundary conditions are described as follows

on the wall:	$u=v=0,\quad \bar{\lambda}\frac{\partial T}{\partial r}=\dot{q}$
on the symmetric axis:	$\frac{\partial u}{\partial r}=v=0,\quad \frac{\partial T}{\partial r}=0$
at the inlet:	$u=u_{in},\quad v=0,\quad p=p_{in},\quad \rho=\rho_{in},\quad T=T_{in}$
at the outlet:	$p=p_{out}$

The values of velocity, pressure, temperature and density at the inlet are evaluated by the method presented by Kariki [17] as described below. For the cells adjacent to the symmetric axis, pressure of the n-th cell from the tube inlet is expressed as p_n. At the time t, pressure of the cell adjacent to the inlet, $(p_{in})_{guess}$, is extrapolated from p_2 and p_3. Then using this $(p_{in})_{guess}$ and $(p_1)_{old}$ at the time t, the inlet pressure p_{in} at the time $t+\Delta t$ is calculated as

$$p_{in}=\omega(p_1)_{old}+(1-\omega)(p_{in})_{guess} \tag{17}$$

where ω is relaxation factor and the value of 0.9 is chosen in this paper. Assuming isentropic change from stagnation point to the tube inlet, ρ_{in}, T_{in} and u_{in} at the time $t+\Delta t$ are calculated using p_{in} of Eq. (17) as

$$\frac{p_{in}}{p_{stg}} = \left(\frac{\rho_{in}}{\rho_{stg}}\right)^{\gamma} = \left(\frac{T_{in}}{T_{stg}}\right)^{\gamma/\gamma-1} \tag{18}$$

$$u_{in} = \sqrt{\frac{2\gamma R T_{stg}}{\gamma-1}\left\{1-\left(\frac{p_{in}}{p_{stg}}\right)^{(\gamma-1)/\gamma}\right\}} \tag{19}$$

k and ε at the inlet is determined as follows

$$k_{in} = \frac{3}{2}(t_u\, u_{in})^2 \tag{20}$$

$$\varepsilon_{in} = 0.1 k_{in}^2 \tag{21}$$

where t_u is ranges from 1% to 6%.

2.4. Dimensionless variables

Attention will now be focused on the calculation of the Reynolds and Mach numbers that will be defined as

$$\mathrm{Re} = \frac{2\dot{m}}{\mu} = \frac{\rho_{ave} u_{ave} D}{\mu}, \quad \mathrm{Ma} = \frac{u_{ave}}{\sqrt{\gamma(\gamma-1)i_{ave}}} \tag{22}$$

where $\dot{m}$ is the mass flow rate per unit depth and D is the tube diameter. u_{ave}, ρ_{ave} and i_{ave} are the average velocity, density and specific internal energy at a cross-section.

$$u_{ave} = \frac{1}{A}\int u dA, \quad \rho_{ave} = \frac{1}{A}\int \rho u dA \Big/ \int u dA, \quad p_{ave} = \frac{1}{A}\int p dA, \quad i_{ave} = \frac{1}{\gamma-1}\frac{p_{ave}}{\rho_{ave}} \tag{23}$$

The product of friction factor and Reynolds number is called Poiseuille number. The friction factors based on the Darcy's and Fanning definitions will be introduced. The Darcy friction factor is defined as

$$f_d = \frac{-2D}{\rho_{ave} u_{ave}^2}\left(\frac{dp_{ave}}{dx}\right) \tag{24}$$

The modified Fanning friction factors (four times of Fanning friction factor) is based on the wall shear stress and is defined as

$$f_f = \frac{4\tau_w}{(1/2)\rho_{ave} u_{ave}^2} = 2D\left(\frac{dp_{ave}}{dx}\right)\left\{\frac{1}{p_{ave}} - \frac{1}{\rho_{ave} u_{ave}^2}\right\} \tag{25}$$

2.5. Numerical solution

The numerical methodology is based on the Arbitrary-Lagrangian-Eulerian (ALE) method proposed by Amsden et al. [18]. The details of the ALE method are documented in the literature and will not be given here. The computational domain is divided into quadrilateral cells. The velocity components are defined at the vertices of the cell and other variables such as pressures, specific internal energy and density are assigned at the cell centers. The number of cells in the *x*-direction was 200. The cell size gradually increased in the x-direction to the mid of the tube and it gradually decreases to the outlet of the tube. The number of cells in *r*-direction was fixed at 40 for all the components. The ALE method

Table 1 Tube diameter, length, p_{stg} Re and Ma

#	D (μm)	L (m)	p_{stg} (kPa)	p_{out} (kPa)	Re	Ma_{in}	Ma_{out}	flow
1	200	0.04	1450	1400	4497	0.070	0.075	slow
2			300	100	2947	0.228	0.660	fast
3			350		3575	0.238	0.778	
4			400		4208	0.246	0.889	
5	400	0.08	200	100	3770	0.218	0.446	fast
6			250		5180	0.242	0.591	
7			300		6541	0.255	0.725	
8			350		7862	0.264	0.846	
9			400		9143	0.269	0.951	

is a time marching method. The value of 10^{-4} was used for convergence criterion of Newton-Raphson iteration in the interior loop of the ALE method.

3. Results and discussion

The computations were performed for the tube with the constant heat flux of $\dot{q}=10^2$, 10^3 and 10^4 W/m^2. The working fluid was nitrogen and it was assumed to be ideal gas. The thermo-physical properties of $R = 296.7$ J·(kg·K)$^{-1}$, $\gamma = 1.399$, $\mu = 1.787\times10^{-5}$ Pa·s and $\lambda = 0.0260$ W·(m·K)$^{-1}$ at 300K were used for the computations. The diameter of the tube was 200 and 400 μm and the aspect ratio of the tube height and length is 200. The stagnation temperature was kept at $T_{stg} = 300$ K. The stagnation pressure, p_{stg} was chosen in such away that the Mach number at the exit ranges from 0.1 to 1.0. The outlet pressure maintained at atmospheric condition, $p_{out} = 100$ kPa. Additionally, in order to obtain turbulent slow flow, the higher outlet pressure maintained with the 1400 kPa for D=200 μm was computed. The tube diameter, the tube length, the stagnation pressure and the corresponding Reynolds & Mach numbers at the inlet and outlet for $\dot{q}=10^4$ W/m^2 are listed in table 1. The Reynolds number obtained ranges from 2947 to 9143, and the Mach number at the outlet ranges from 0.070 to 0.951 widely.

3.1. Velocity vectors and contour plot of temperature

Velocity vectors for the case #1 and #4 in table 1 are presented in Figure 2. Contour plots of temperature are also presented in Figure 3. These are typical velocity vectors and temperature contour plots for the combination of slow and fast flows. Figure 2 shows the velocity vectors of gas flow with uniform velocity at the inlet. The flows are turbulent since the shape of the velocity profile except near the inlet is almost flat. Also, obtained Reynolds number is well lager than the critical Reynolds number. The gaseous flow is accelerated in a microtube. Therefore, Mach number at the outlet is greater than that at the inlet, $Ma_{in}<Ma_{out}$. The flow whose Ma at the outlet is less than 0.3 is called as "slow flow" and the flow whose Ma at the outlet is greater than 0.3 is called as "fast flow". As can be seen in Figure 3 (a), in the case of the slow flow ($Ma_{out} < 0.3$), the temperature rises gradually along the tubes through the influence of the constant heat flux. This is the similar temperature contour to that of the incompressible flow since the temperature contour begins to develop along the tube length with parabolic curves depending on the constant heat flux. On the other hand, in the case of the fast

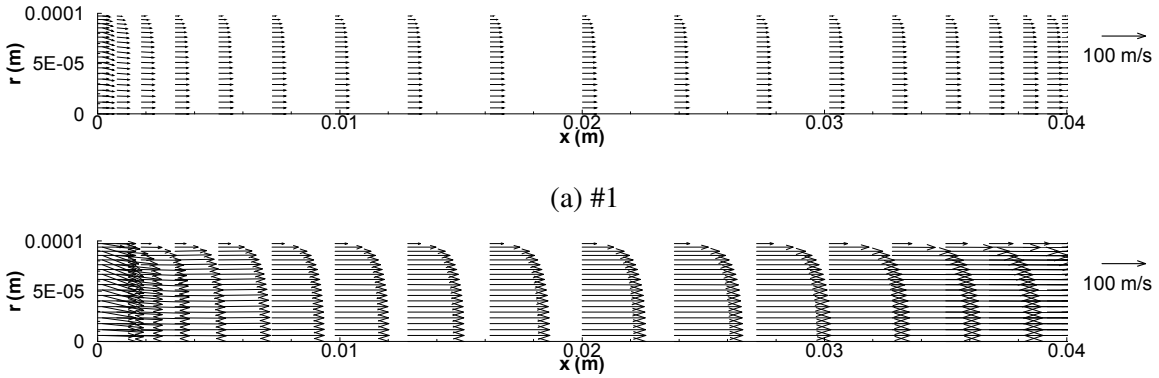

(a) #1

(b) #4

Figure 2. Velocity vector for slow (a) and fast flow (b)

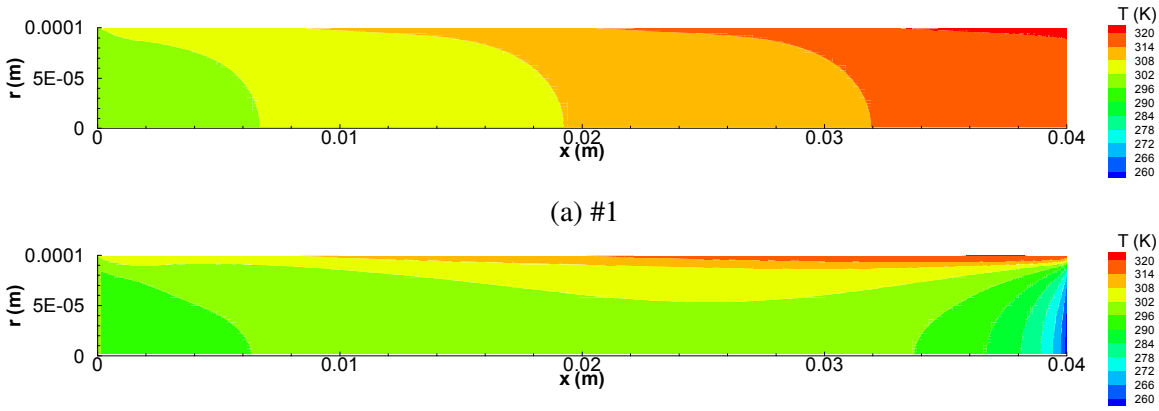

(a) #1

(b) #4

Figure 3. Contour plots of temperature for slow (a) and fast flow (b)

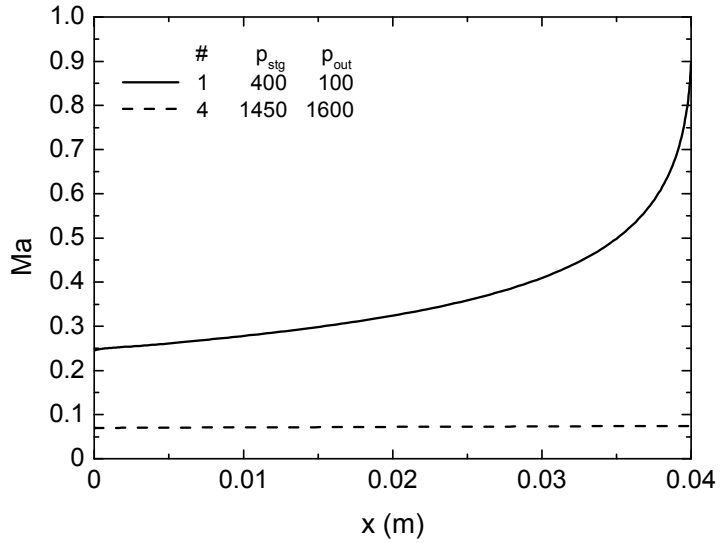

Figure 4 Ma as a function *x*

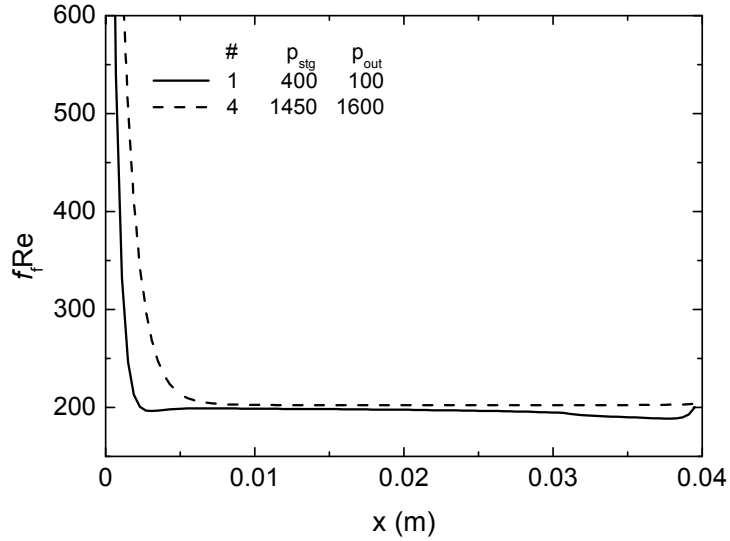

(a) $f_f \cdot$Re

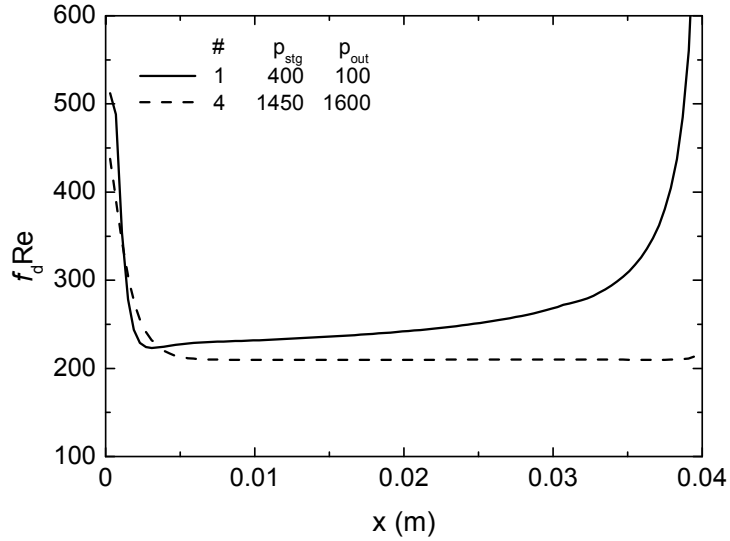

(b) $f_d \cdot$Re

Figure 5 $f \cdot$Re as a function of x

flow ($Ma_{out} > 0.3$), the temperature fall can be seen near the outlet due to the energy conversion into the kinetic energy caused by the flow acceleration in the core region of the tube (Figure 3 (b)). The wall temperature decreases approaching to the outlet due to the temperature fall in the core region. This is the typical temperature contour of the compressible flow.

3.2. Mach number and friction factor

The product of the friction factor and Reynolds number, $f_f \cdot$Re and $f_d \cdot$Re of two cases for Figures 2 and 3 are plotted as a function of x in Figures 4 (a) and (b), respectively. Corresponding Mach numbers are also plotted in Figure 5. As can be seen in Figures 4 (a) and (b), the tube can be divided into two

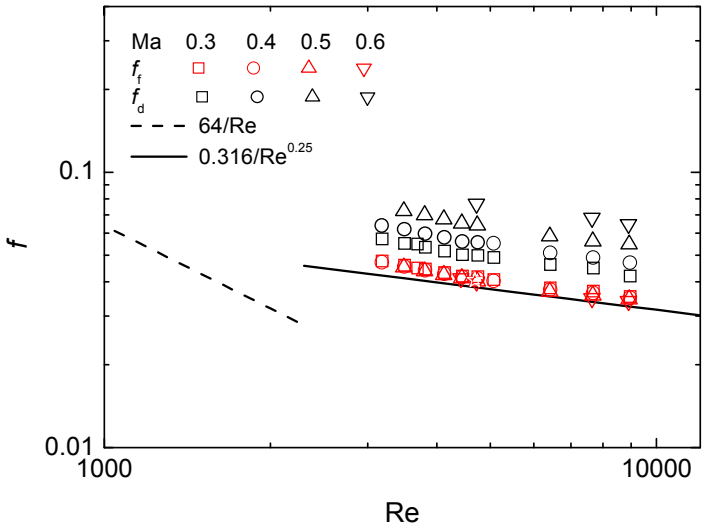

Figure 6 f on Moody chart

regions. The region where the friction factor decrease sharply for both cases can be considered the entrance region. In the case slow flow, the region after the entrance region can be considered as fully developed region. However, in the case of fast flow, the region after the entrance region can be considered as the quasi-fully developed region. Then the Mach number increases along the tube due to acceleration of the flow. The value of $f_f \cdot$Re of fast flow almost coincide with that of slow flow since the viscous wall friction loss for turbulent flow depends on Reynolds number. The value of $f_d \cdot$Re of fast flow is higher than that of slow flow since $f_d \cdot$Re includes the acceleration loss. And the value of $f_f \cdot$Re of fast flow agrees with that of slow flow since the $f_f \cdot$Re do not include flow acceleration loss. The f_f and f_d obtained for all case of the present numerical calculations plotted as a function on Moody chart in Figure 6. Then, the f_f and f_d at the locations where Mach number indicated just 0.3, 0.4, 0.5, 0.6 and 0.7 are extracted from numerical results. The solid line and dashed line represent conventional correlation of friction factor for incompressible flow (f = 64/Re for laminar flow and f = 0.316Re$^{-0.25}$ (Blasius correlation) for turbulent flow). f_f is almost coincide with conventional value given by Blasius correlation. As can be seen in Figure 2, gradient of the normalized velocity at the wall is almost constant even if Mach number changes, so f_f depends only on Reynolds number. However, the plotted values of f_d at constant Mach number are aligned on a straight lines. These lines are parallel to the line of Blasius correlation (f = 0.316Re$^{-0.25}$) and shift upwards as Mach number increases. The ratio of f_d to f_f or Blasius correlation is dependent on only Mach number and independent on Reynolds number.

3.3. Wall temperatue and Nusselt number of incompressible flow

In the case of the incompressible flow, the local Nusselt number, based on the temperature difference between the wall and the bulk temperatures, of a simultaneously developing flow in a duct with the constant heat flux is defined as

$$\mathrm{Nu}_x = \frac{\dot{q}D}{(T_w - T_b)k} \tag{26}$$

If the flow is incompressible, the bulk temperature is expressed by the function of x as

$$T_b = T_{in} + \frac{2\dot{q}x}{\int \rho C_p u dA} \tag{27}$$

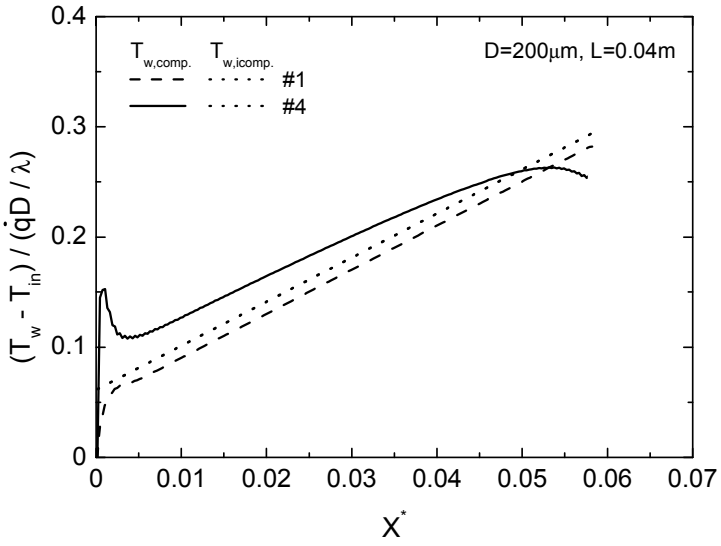

Figure 7 Dimensionless wall temperature as a function of X^*

The wall temperature of an incompressible flow in a duct is expressed as a function of a local Nusselt number and the location as

$$T_w = \left(4X^* + \frac{1}{Nu_x}\right)\left(\frac{\dot{q}D}{k}\right) + T_{in} \tag{28}$$

where X^* is the inverse of Graetz number defined by

$$X^* = \frac{x}{D\,Re\,Pr} \tag{29}$$

Equation (28) can be rewritten as

$$\frac{T_w - T_{in}}{\dot{q}\,D\,/k} = 4X^* + \frac{1}{Nu_x} \tag{30}$$

The dimensionless wall temperature of an incompressible flow in a duct is a function of X^* and Nu_x. The turbulent heat transfer characteristics for incompressible duct flows has been investigated by many researchers and Nusselt numbers were reported in literatures (e.g., Kays and Crawford [19]). In the present study, the obtained Nu for the turbulent fully developed flow by Kays and Crawford [19] defined by

$$Nu = 0.022\,Re^{0.8}Pr^{0.5} \tag{31}$$

was used for the calculation of the wall temperature for the incompressible flow.

3.4. Estimation of wall temperature

The dimensionless wall temperature, $(T_w - T_{in})/(\dot{q}\,D/k)$, for two cases of the tubes of D=200 μm for $\dot{q}=10^4$ W/m^2 is plotted as a function of X^* in Figure. 7. The dimensionless wall temperature for the incompressible flow obtained by Equation (30) is also plotted in the figure. As can be seen in Figure 2 in the case of slow flow (#1), the dimensionless wall temperature increases along the dimensionless length and it coincides with that of incompressible flow. On the other hand, in the case of fast flow (#4), the dimensionless wall temperature increases gradually along the dimensionless length and level off and decreases quickly approaching to the outlet due to the conversion of the thermal energy into the kinetic energy. The qualitative same tendency can be seen for the tubes with D=400μm. Therefore, in the case of fast flow (Ma_{out}>0.3), the wall temperature of the gas flow in the microtube

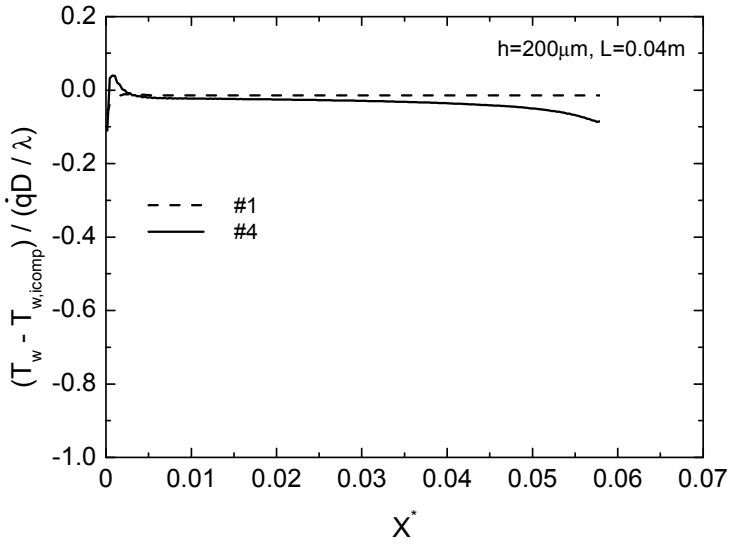

(a) Dimensionless wall temperature difference

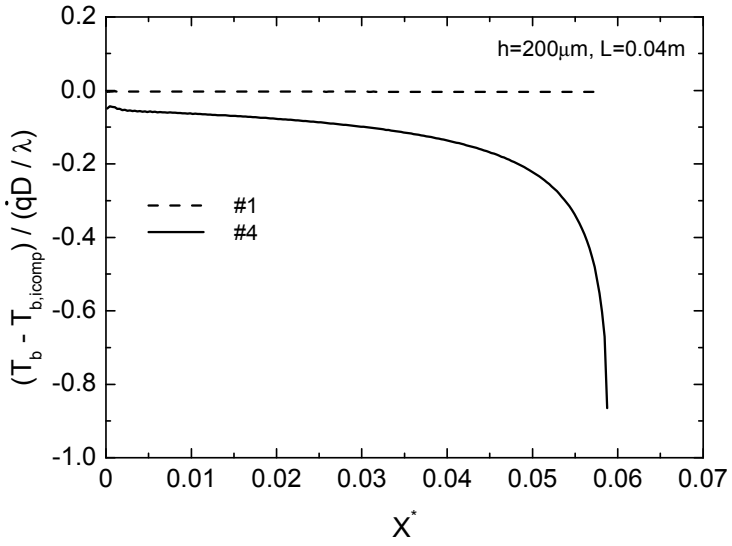

(b) Dimensionless bulk temperature difference

Figure 8 Dimensionless wall and bulk temperature differences as a function of X^*

can not be directly estimated from the correlation for the incompressible flow. In addition, the computed dimensionless temperatures of several cases are slightly higher than that of the incompressible flow near the inlet since the effect of viscous dissipation is relatively prevalent before the flow acceleration occurs.

The dimensionless wall temperature differences, $(T_w - T_{w,icomp})/(\dot{q}D/k)$, between the gas flow and incompressible flow for two cases of the tubes of D=200 μm for $\dot{q}=10^4$ W/m^2 are plotted as a function of X^* in Figure 8 (a). Also, the dimensionless bulk temperature differences, $(T_b - T_{b,icomp})/(\dot{q}D/k)$, between the gas flow and incompressible flow are plotted as a function of X^* in Figure 8 (b). In the case of slow flow, the dimensionless wall and bulk temperatures coincide with those of incompressible flow. Therefore, there is no difference between them as shown in Figure 8 (a) and (b). On the other

hand, in the case of fast flow, the dimensionless wall and bulk temperature difference decreases approaching to the outlet.

Note that the bulk temperature difference between the gas flow and incompressible flow represents the dynamic temperature of the fluid, T_k, defined as

$$T_k = \frac{\int \rho u \frac{u^2}{2} dA}{\int \rho C_p u dA} \tag{32}$$

The gas temperature decreases near the outlet due to the energy conversion into the kinetic energy as shown in Figure 3. If the thermal conductivity of the gas is extremely high, the wall temperature falls corresponding to the fall of the bulk temperature. However, in actual situation, the thermal conductivity of the gas is low, therefore the fall of the wall temperature is smaller than that of the bulk temperature as shown in Figure 8 (a) and (b). Then, the ratio of wall temperature difference between the gaseous flow and incompressible flow and the dynamic temperature, ζ is defined as

$$\zeta = \frac{T_{w,icomp} - T_w}{T_k} \tag{33}$$

The ratio, ζ calculated from Equation (33) for fast flow cases of Table 1 is plotted in Figure 9 as a function of the Mach number at the outlet. The ratio calculated for $\dot{q}=10^2$ W/m^2 and $\dot{q}=10^3$ W/m^2 are plotted in the figure. For the case of slow flow, the flow can be assumed to be an incompressible flow, and the temperature differences between the wall temperature and those of incompressible flow and the dynamic temperature are quite small, therefore, it is not plotted in Figure 9. The dashed line represent the ratio for laminar flow obtained by the previous study (Hong et al. [20]). The ratio, ζ is independent of hydraulic diameter and decreases with increasing the Ma at the outlet. Eq. (33) can be rewritten as

$$T_w = T_{w,icomp} - \zeta\, T_k \tag{34}$$

Then, the wall temperature of tubes with constant heat flux can be predicted from the wall temperature of the incompressible flow, the ratio, ζ and the dynamic temperature. However, the ratios for $\dot{q}=10^2$ W/m^2 and $\dot{q}=10^3$ W/m^2 scattered since their heat flux are relatively not large for the turbulent fast flow ($Ma_{out} > 0.3$) of $D \geq 200\mu m$.

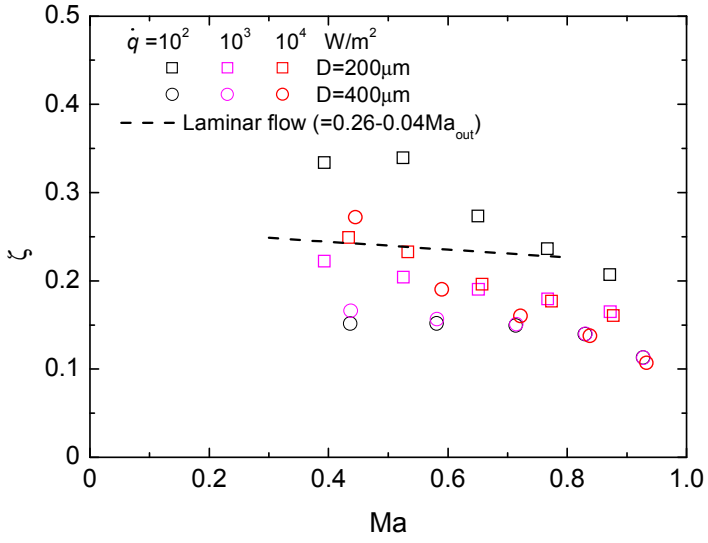

Figure 9 ζ as a function of Ma_{out}

4. Concluding remarks

Two-dimensional compressible momentum and energy equations are solved to obtain the heat transfer characteristics of turbulent gas flow in microtubes with constant hest flux. The Lam-bremhorst Low Reynolds number turbulence model was adopted to simulate turbulent flow cases. The following conclusions are obtained.

(1) For turbulent flow, Fanning friction factor, f_f is almost equal to the value given by Blasius correlation. However, Darcy friction factor, f_d with acceleration loss is higher than f_f or Blasius correlation.

(2) In the case of slow flow, the identical temperature profiles normalized by heat flux are obtained with those of incompressible flow. However, in the case of fast flow in a microtube, different temperature profiles are obtained.

(3) The wall temperature of a microtube can be predicted from the wall temperature of the incompressible flow, the ratio, ζ and the dynamic temperature.

$$T_w = T_{w,icomp} - \zeta\, T_k$$

5. References

[1] Asako, Y., Nakayama, K. and Shinozuka, T., 2005, Effect of Compressibility on Gaseous Flows in Micro-tube, *International Journal of Heat and Mass Transfer*, vol. 48, pp. 4985-4994.

[2] Wu, P. and Little, W.A., 1984, Measurement of the Heat Transfer Characteristics of Gas Flow in Fine Channel Heat Exchanger used for Microminiature Refrigerators, *Cryogenics* vol. 24, pp. 415-420.

[3] Chen, C.S. and Kuo, W.J., 2004, Numerical Study of Compressible Turbulent Flow in Microtubes, *Numerical Heat Transfer*, *Part A*. Vol. 45, pp. 85-99.

[4] Hara, K, Inoue, M and Furukawa, M., 2007, Heat Transfer in Mini-Channel Gaseous Cooling, *J. Environ. Eng*., Vol. 2(3), pp. 525-534.

[5] Turner, S.E., Asako, Y. and Faghri, M., 2007, Convection Heat Transfer in Microchannels with High Speed Gas Flow, *Journal of Heat Transfer*, 129, pp.319-328.

[6] Asako, Y., 2004, Heat transfer characteristics of gaseous flow in a Micro-tube, *Thermal science & engineering*, 12(5), pp. 31-37.

[7] Asako, Y. and Toriyama, H., 2005, Heat Transfer Characteristics of Gaseous Flows in Micro-channels, *Microscale Thermophysical Engineering*, 9, pp. 15-31.

[8] Hong, C. and Asako, A., 2007, Heat Transfer Characteristics of Gaseous Flows In a Microchannel and a Micortube With Constant Wall Temperature, *Numerical Heat Transfer, Part A* , 52, pp. 219-238.

[9] Hong, C., Uchida, Y., Yamamoto, T., Asako, Y. and Suzuki, K., 2010, Heat Transfer Characteristics of Turbulent Gas Flow through Micro-Tubes, 2010 ASME International Heat Transfer Conference, Washington, DC, USA, IHTC14-22355.

[10] Chen, C., Lin, T., Yang, C. and Kandlikar, S.G., 2011, An experimental investigation on heat transfer characteristics of air and CO_2 in microtubes, *Ninth International Conference on Nanochannels, Microchannels, and Minichannels*, Paper No. ICNMM2011-58102.

[11] Yang, Y., Morini, G.L., Chalabi, H. and Lorenzini, M., 2011, Experimental Nusselt number determination for gas flows through commercial microtubes, *Third GASMEMS Workshop*, Paper No. GASMEMS11-21.

[12] Hong, C., Yamamoto, T., Asako Y. and Suzuki, K., 2012, Heat Transfer Characteristics of Compressible Laminar Flow Through Microtubes, *Journal of Heat Transfer*, Vol. 134, p. 011602 (8 page)

[13] Isobe, K., Hong, C., Asako, Y. and Ueno, I., 2011, Heat transfer characteristics of gas flow in micro-tubes with constant wall temperature, 4th International Conference on Heat Transfer and Fluid Flow in microscale, HTFFM-IV-068.
[14] Patel, C.V., Rodi, W. and Scheuerer, G., 1985, Turbulent Models for Near-Wall and Low Reynolds Number Flows: A Review, *AIAA Journal*, Vol.23 , pp. 1308-1319.
[15] Lam, C.K.G. and Bremhorst, K., 1981, A Modified Form of the k-ε Model for Predicting Wall Turbulence, *Transactions of American Society of Mechanical Engineers*, Vol. 103, pp. 456-460.
[16] Murakami, S. and Asako, Y., 2011, Local Friction Factor of Compressible Laminar or Turbulent Flow in Micro-Tubes, ASME 2011 9th International Conference on Nanochannels, Microchannels and Minichannels, ICNMM2011-58036.
[17] Kariki, C.K., 1986, A Calculation Procedure for Viscous Flows at All Speeds in Complex Geometries, PhD Thesis, *University of Minnesota*.
[18] Amsden, A.A., Ruppel, H.M. and Hire, C.W., 1980, SALE a Simplified ALE computer Program for fluid Flow at all Speeds, Los Alamos Scientific Laboratory Report No. LA-8095.
[19] Kays, W.M. and Crawford, M.E., 1980, Convective heat and Mass Transfer, 2nd ed. New York McGraw-Hill.
[20] Hong, C., Asako, A. and Lee, J-H., 2007, Heat transfer characteristics of gaseous flows in micro-channel with constant heat flux, *International Journal of Thermal Sciences*, Vol. 46, pp. 1153-1162.